Supporting Information

Inorganic nanocrystal-dynamic porous polymer assemblies with effective energy transfer for sensitive diagnosis of urine copper

Xujiao Ma, Yajie Yang, Rongchen Ma, Yunfeng Zhang, Xiaoqin Zou, Shoujun Zhu, Xin Ge, Ye Yuan,* Wei Zhang,* and Guangshan Zhu*

Xujiao Ma, Yajie Yang, Rongchen Ma, Yunfeng Zhang, Xiaoqin Zou, Ye Yuan, and Guangshan Zhu
Key Laboratory of Polyoxometalate Science of Ministry of Education, Northeast Normal University, Renmin Avenue, Changchun, 130024, China
E-mail: Yuany101@nenu.edu.cn; zhugs@nenu.edu.cn
Shoujun Zhu
State Key Laboratory of Supramolecular Structure and Materials, College of Chemistry, Jilin University, Changchun 130012, China.
Xin Ge and Wei Zhang
Key Laboratory of Automobile Materials MOE, School of Materials Science & Engineering, Electron Microscopy Center, and International Center of Future Science, Jilin University, Changchun 130012, China
E-mail: weizhang@jlu.edu.cn

Chemicals.

All reagents were purchased from Sigma-Aldrich or Alfa and used as received unless otherwise indicated. All urine samples were provided by the affiliated hospital of Northeast Normal University. Ethical approval and informed consent was obtained from all patients before conducting the experiments. All experiments were performed in compliance with the relevant laws and institutional guidelines. The protocol of study was approved by the Key Laboratory of Polyoxometalate Science of Ministry of Education and Northeast Normal University, respectively. The urine samples were also sterilized before taking them out of the hospital and all the patients are from similar backgrounds.

Measurements.

Powder X-ray diffraction (XRD) measurements were performed on a Smartlab instrument with Cu Kα (λ=1.5418 Å) radiation and X-Ray 40 kV/30 mA over the angular range 2θ 4°–40° at a scan rate of 10° min^{-1}. SEM was acquired by using JSM 6700 and Hitachi SU8000 scanning electron microscopes at 3 kV and 5 μA. EDAX spectrum was recorded by TEAM EDS (EDAX, USA) on HITACHI SU8010 SEM. We dispersed the sample (1 mg) in 2 mL ethanol by ultrasound and placed the dispersed droplets on a clean silicon wafer. After the ethanol volatilized, the silicon wafer supporting sample was kept at 60 ℃ for 12h and then tested by SEM. TEM was performed on the JEM Grand ARM300F at 200 kV from Electron Microscopy Center, and School of Materials Science & Engineering, Jilin University, China. We dispersed the sample (1 mg) in 5 mL ethanol by ultrasound and placed the dispersed droplets on a clean microgrid. After the ethanol volatilized, the microgrid supporting sample was kept at 60 ℃ for 12 h and then tested by TEM. FT-IR measurements were performed on the Nicolet Impact 410 Fourier transforms infrared spectrometer. N_2 adsorption isotherms and pore size distribution were obtained on the Micromeritics ASAP 2010M analyzer. Photoluminescence (PL) spectra, time-resolved fluorescence spectra,

and quantum fluorescence efficiency for CD@COFs were obtained using a FLSP920 Edinburgh fluorescence spectrometer. All fluorescence measurements were performed at room temperature. The PL was measured from a Xe lamp. For PLQY measurement, analyte soild was loaded onto the sample holder to fully cover the bottom. Thermogravimetric analysis (TGA) was carried out on a METTLER-TOLEDO TGA/DSC 3+ analyser with a heating rate of 10 ^{o}C min^{-1} under air flow. The X-ray photoelectron spectrum (XPS) was measured by a VG ESCALAB MKIIX-ray photoelectron spectrometer using Mg-Kα as the exciting source (1253.6 eV) and binding energy calibration was based on C_{1s}, N_{1s} and O_{1s}. The solid–state ^{13}C NMR spectra were recorded at an ambient temperature on a Bruker Avance 400 MHz Solid State NMR Spectrometer, operating at frequencies of 125.7 MHz. The sample was contained in a 4 mm ZrO_2 rotor (Bruker) which was mounted in a standard double resonance MAS probe. The ^{13}C chemical shifts were referenced relative to TMS and nitromethane. LSCM images were filmed by Olympus FV-1000.

Preparation of COFs.

Each aldehyde compound (1.2 mmol of functional group) and hydrazine species (1.2 mmol) was added to dioxane (2 mL) and AcOH (0.2 mL, 6 M) in a 10 mL Schlenk tube. The mixtures were sonicated for 10 minutes, followed by the degassing processes of three freeze-pump-thaw cycles under a 77 K liquid nitrogen treatment and were finally sealed under vacuum. After heating at 120 °C for 3 days, a pale yellow solid was obtained, washed for three times with tetrahydrofuran, and then dried under vacuum at 80°C for 10 hours to give COFs.

Preparation of CD@COFs.

10 mg of COFs was placed in a 1.5 mL centrifuge tube, and a high concentration sodium citrate solution (0.5 mL, 25 μM) was added to the system. The mixture was shaken for 2 hours under a constant temperature on a high speed oscillator. The solid obtained by washing with an aqueous solution was

then placed in a muffle furnace and heated (300 °C, 2 hours) to obtain CD@COFs.

Cu^{2+} ion fluorescence detection.

Various nitrates were dissolved in deionized water to obtain the solutions containing Cu^{2+}**,** Ag^{+}, K^{+}, Ba^{2+}, Ca^{2+}, Co^{2+}, Mg^{2+}, Ni^{2+}, Zn^{2+}, Al^{3+} and Fe^{3+} metal ions with a concentration of 0.1 mol L^{-1}. These solutions were used in Cu^{2+} detection experiments. 10 mg CD@BPOF-1 was dispersed ion in 100 mL solution for detection. Each time 30 mL of the dispersion was taken into the cuvette, and photoluminescence measurements were carried out after dropping different concentrations of the metal ion solution. All fluorescence measurements were performed at room temperature.

Urine Cu^{2+} ion detection.

The urine of healthy people was obtained, and additional Cu^{2+} ions were added to simulate the urine of Wilson patients. 1 mg CD@BPOF-1 was added to 1 mL of urine (containing different concentrations of copper ions) to disperse uniformly, filtered onto a circular filter paper and irradiated under an ultraviolet lamp to observe the fluorescence intensity.

Calculations.

Equation (1) was used to obtain the FRET efficiency and equation (2) was used to calculate the EnT rate (K_{EnT}):

$\eta_{EnT} = 1-\tau_{DA}/\tau_{D}$ (1)

$K_{EnT} = 1/\tau_{DA}-1/\tau_{D}$ (2)

where η_{EnT} is the FRET efficiency and τ_{DA} and τ_{D} are the fluorescence lifetimes of a donor in the presence and absence of an acceptor, respectively.

The variation of the PL intensity according to the Cu^{2+} ion concentration was calculated by the Stern-Volmer equation:

$F_0/F = 1+K[Q]$ (3)

where F_0 and F are the FL intensities before and after quenching, respectively; [Q] is

the Cu^{2+} ion concentration.

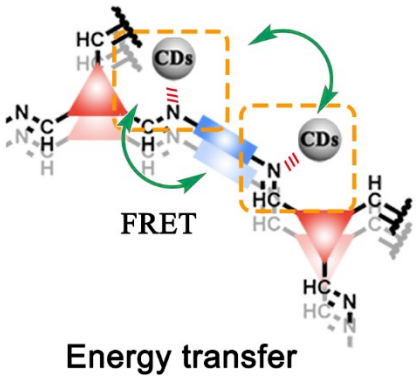

Figure S1. Carbon quantum dots are in-situ polymerized in polymers *via* hydrogen bonding interaction to trigger the energy transfer.

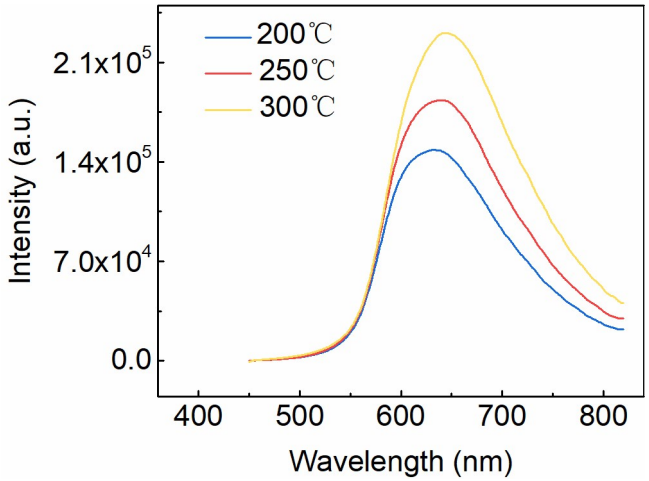

Figure S2. PL emission spectra for CD@BCOF-1 at different temperatures.

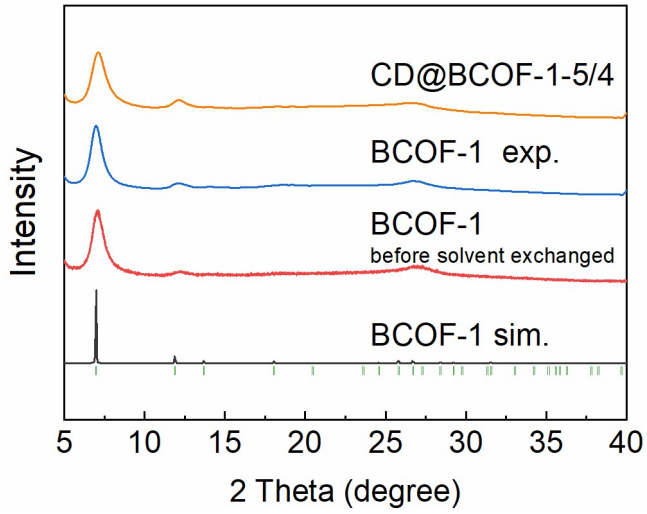

Figure S3. Simulated and experimental PXRD patterns of BCOF-1. PXRD pattern of CD@BCOF-1-5/4.

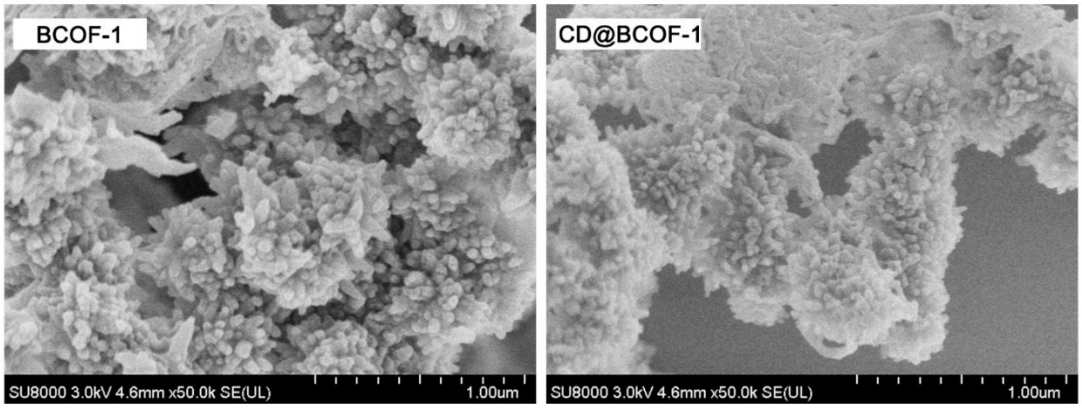

Figure S4. SEM images of BCOF-1 and CD@BCOF-1.

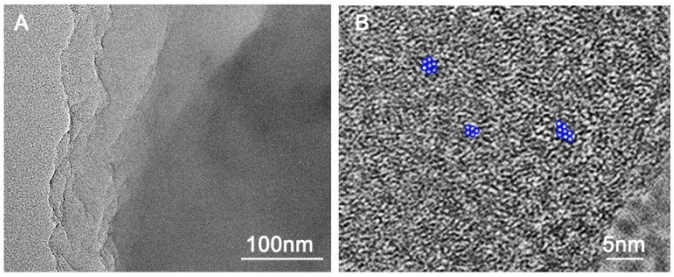

Figure S5. TEM and HRTEM images of BCOF-1.

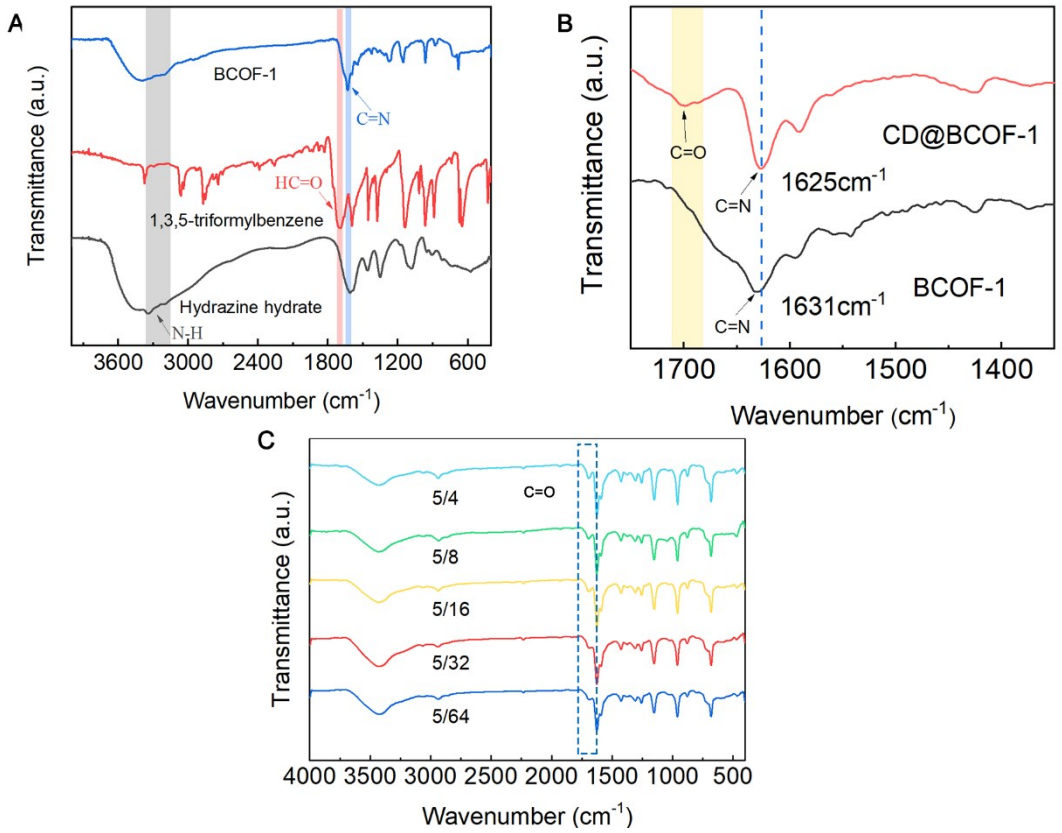

Figure S6. (A) FT-IR spectra for BCOF-1 and the starting materials. (B) FTIR spectra for BCOF-1 (black) and CD@BCOF-1-5/4 (red). (C) FTIR spectra for CD@BCOF-1-*X* (*X* = 5/4, 5/8 5/16, 5/32, 5/64).

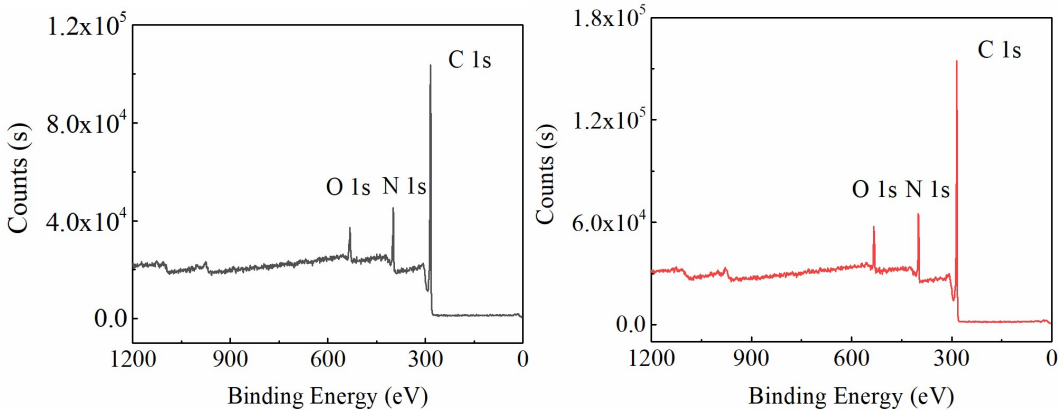

Figure S7. XPS survey of BCOF-1 (left) and CD@BCOF-1 (right).

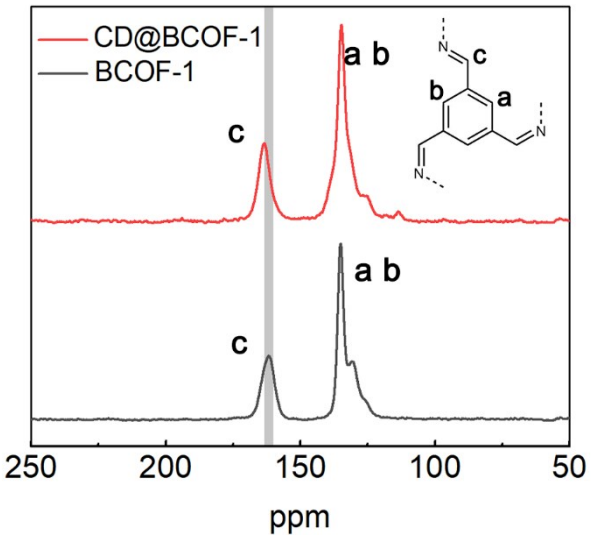

Figure S8. ^{13}C NMR spectra for BCOF-1 and CD@BCOF-1.

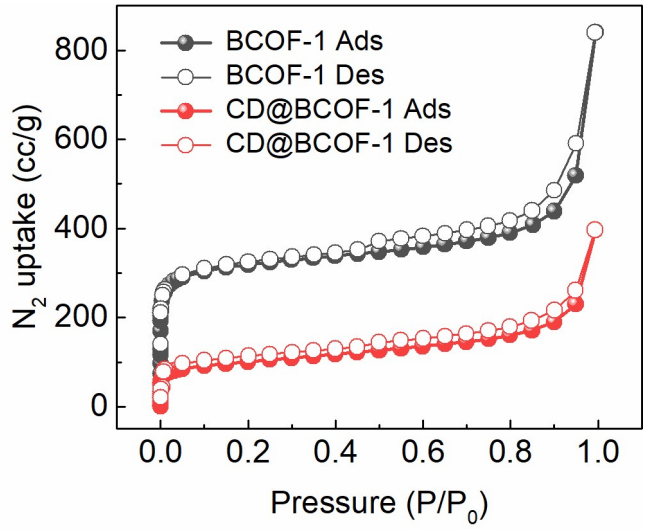

Figure S9. Nitrogen adsorption-desorption isotherms for BCOF-1 and CD@BCOF-1-5/4.

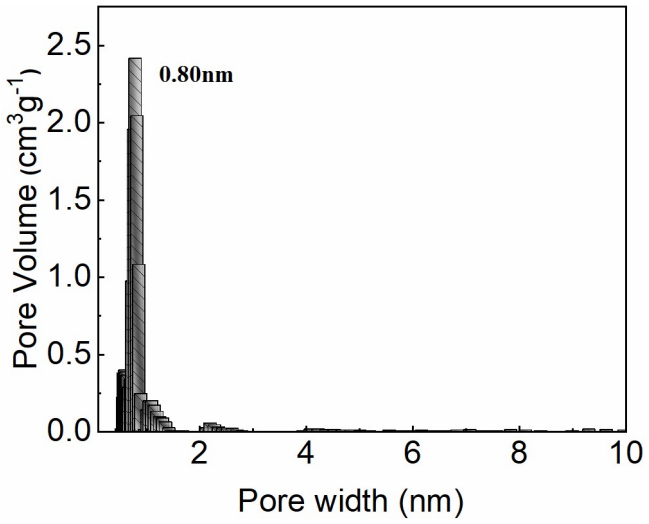

Figure S10. Pore size distribution of BCOF-1 based on NL-DFT model.

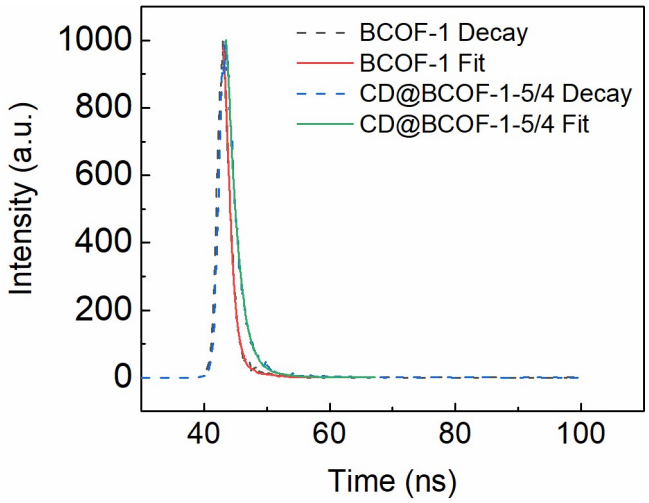

Figure S11. TRPL spectra and the corresponding fitting curves of CD@BCOF-1 and BCOF-1, respectively, under 420 nm excitation.

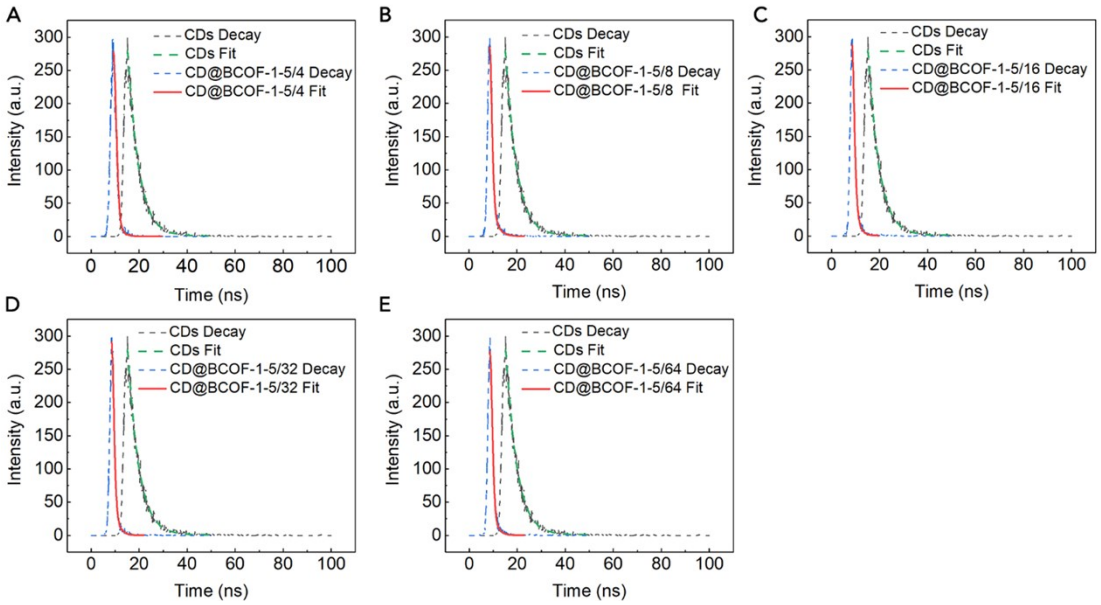

Figure S12. TRPL spectra and the corresponding fitting curves of CD@BCOF-1-X and CDs, respectively, under 380 nm excitation.

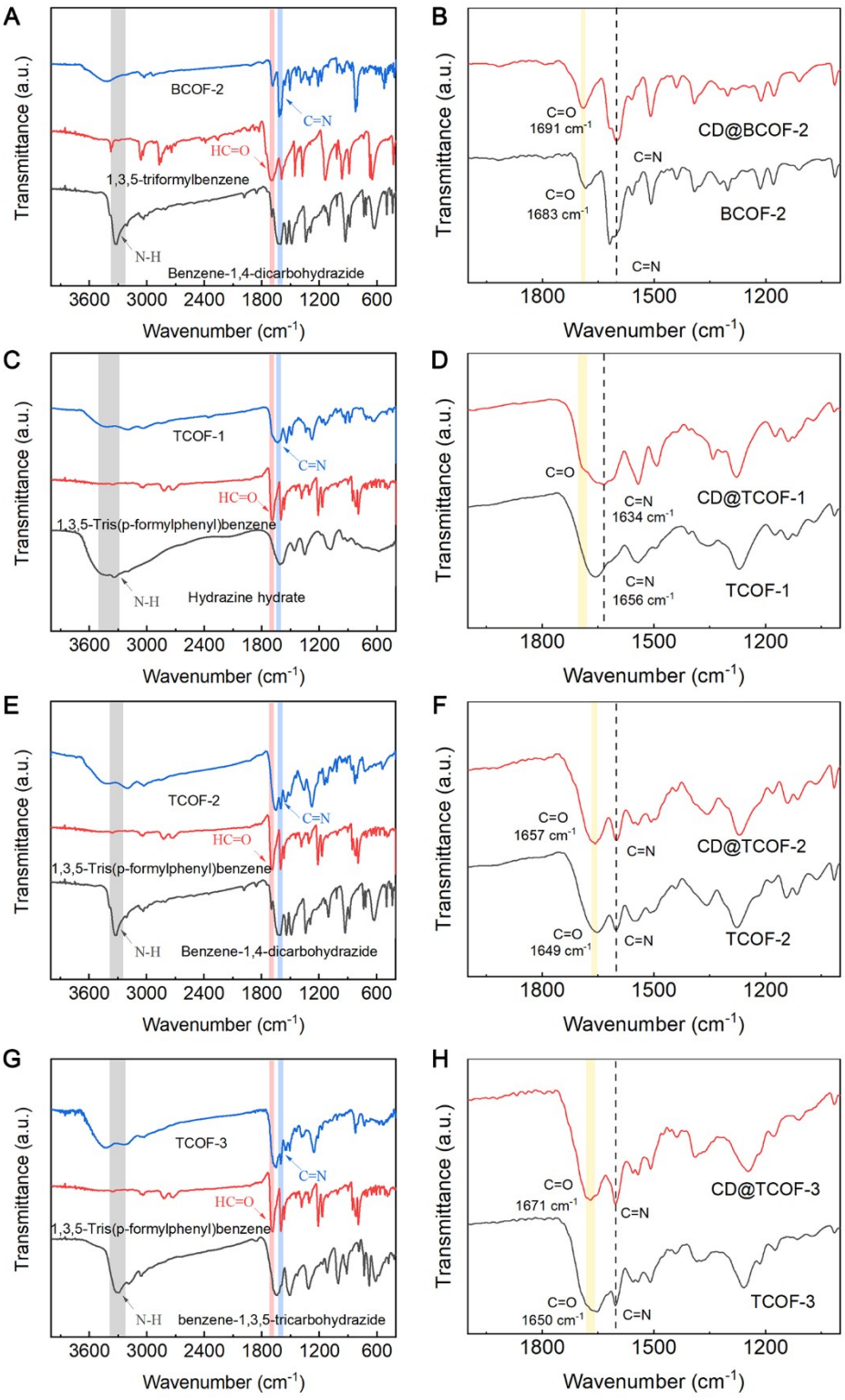

Figure S13. FTIR spectra for COFs, CD@COFs, and starting materials.

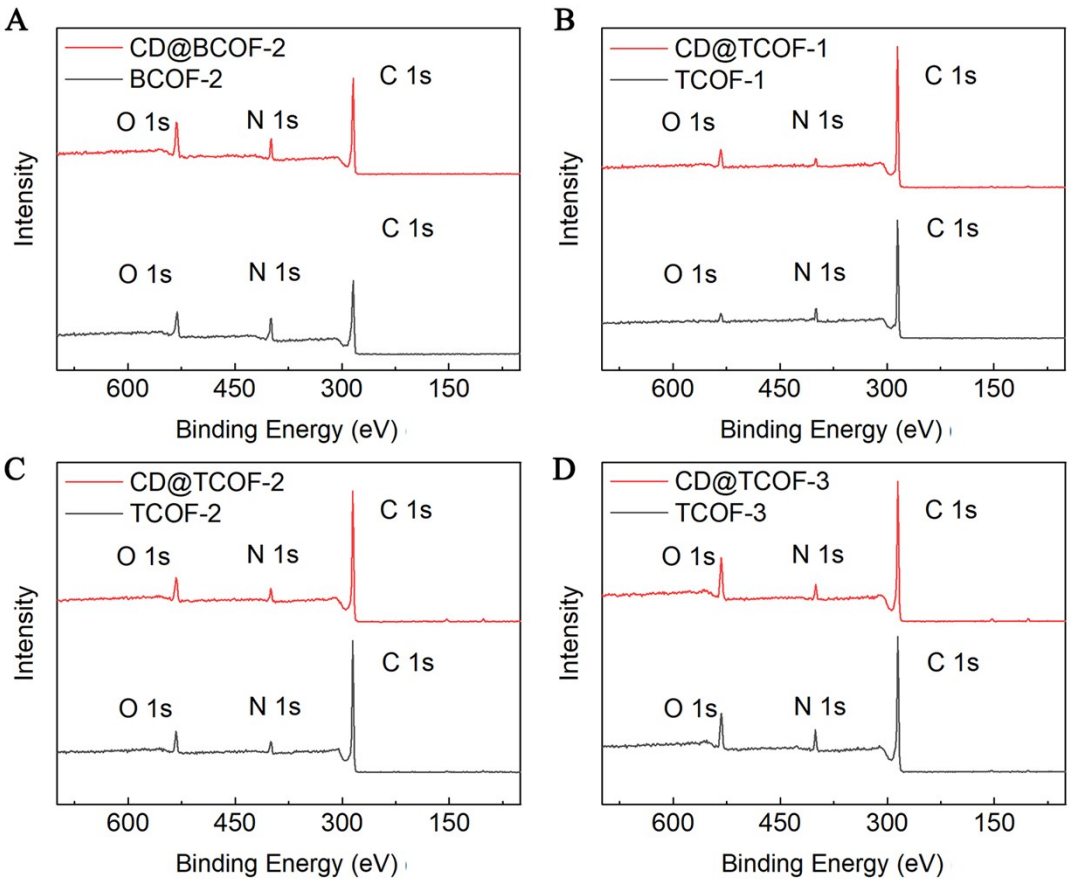

Figure S14. XPS survey of COFs and CD@COFs.

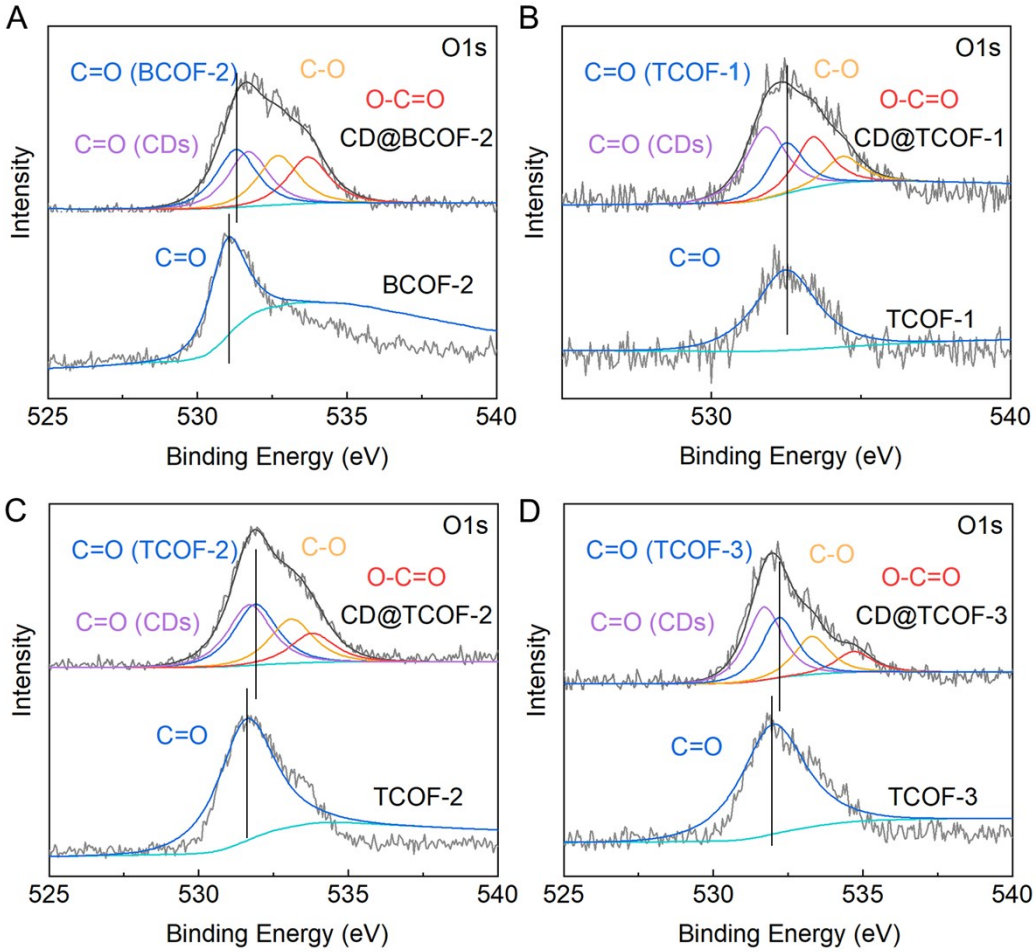

Figure S15. O_{1s} XPS spectra for COFs and CD@COFs.

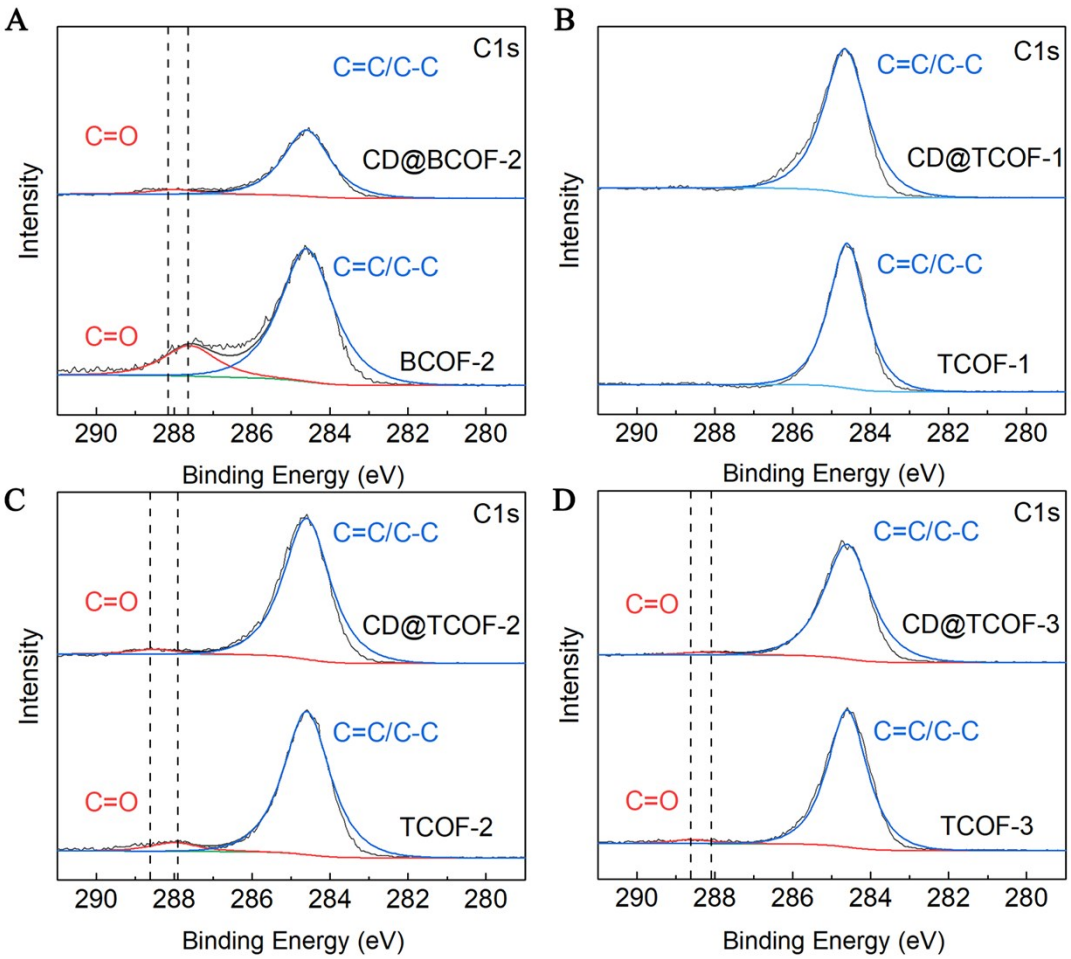

Figure S16. C_{1s}XPS spectra for COFs and CD@COFs.

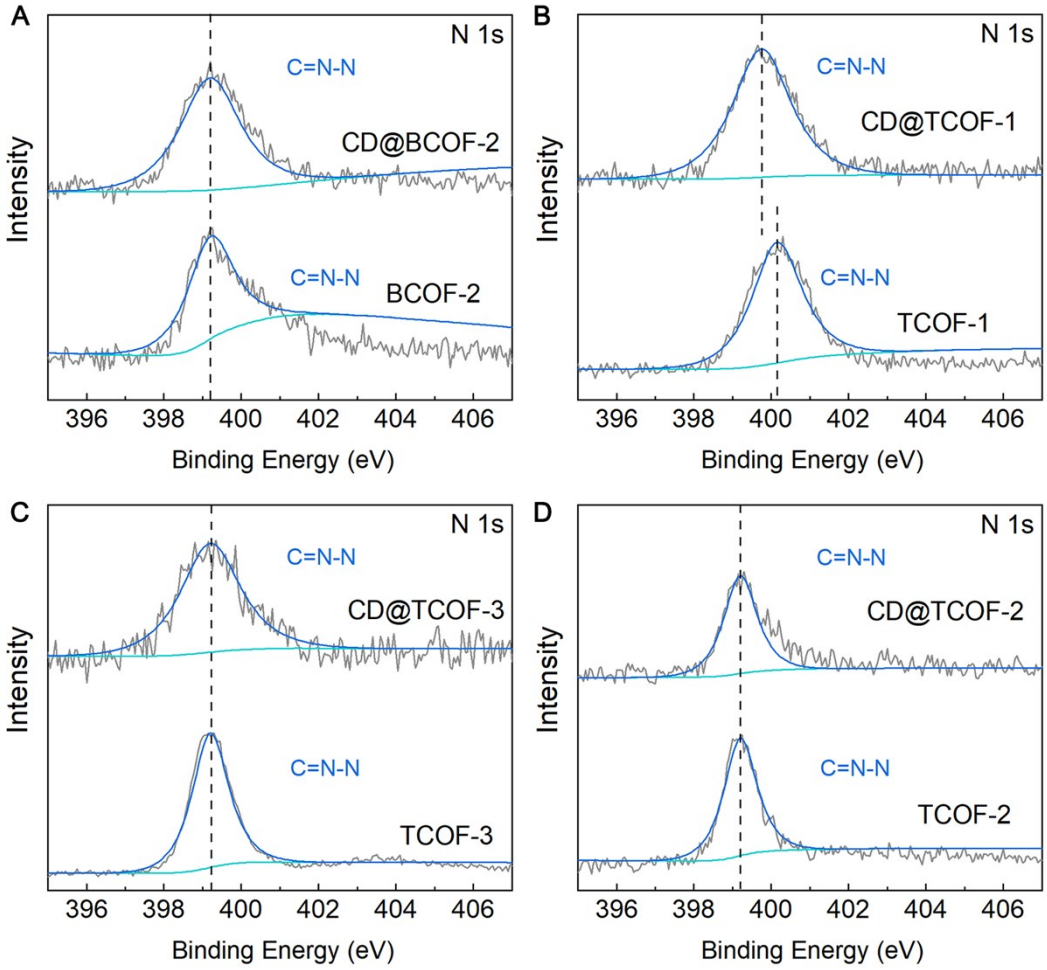

Figure S17. N_{1s} XPS spectra for COFs and CD@COFs.

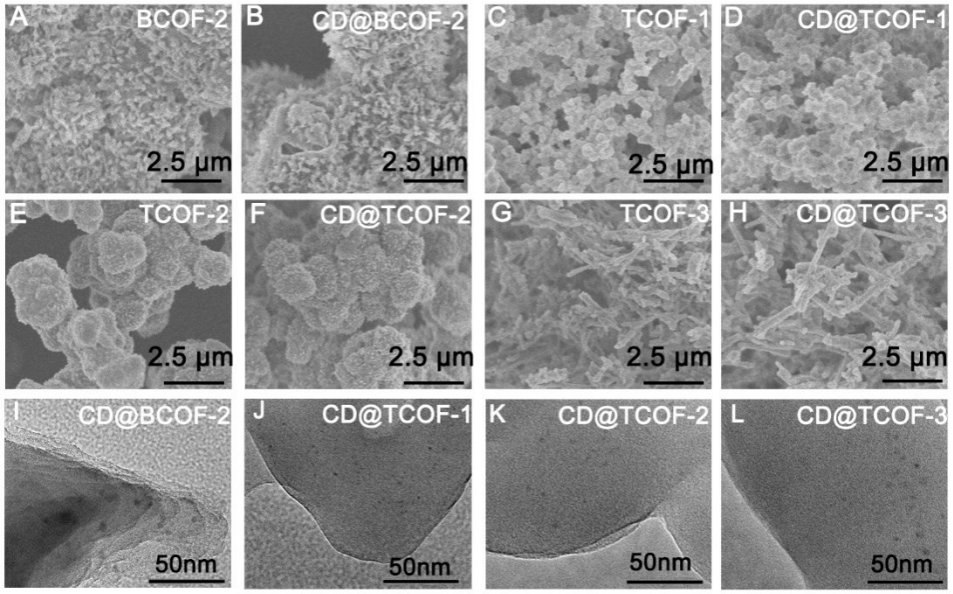

Figure S18. SEM images of COFs and CD@COFs (A-H). TEM images of CD@COFs (I-L).

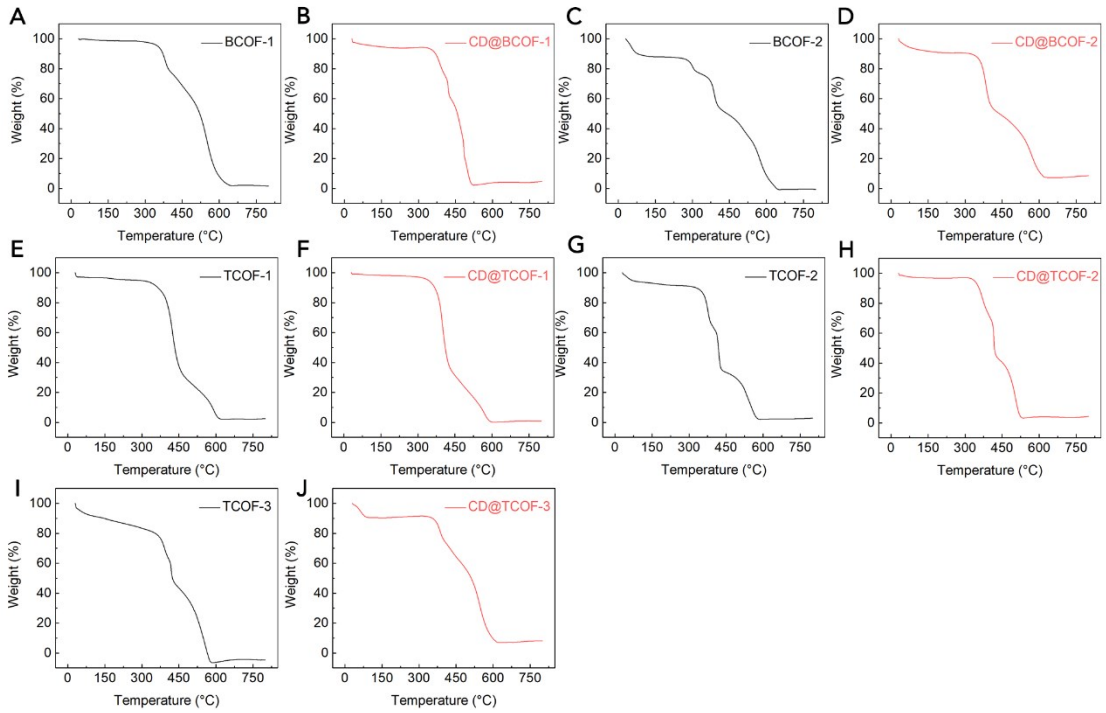

Figure S19. TGA for COFs and CD@COFs under air with a heating rate of 10 °C per minute.

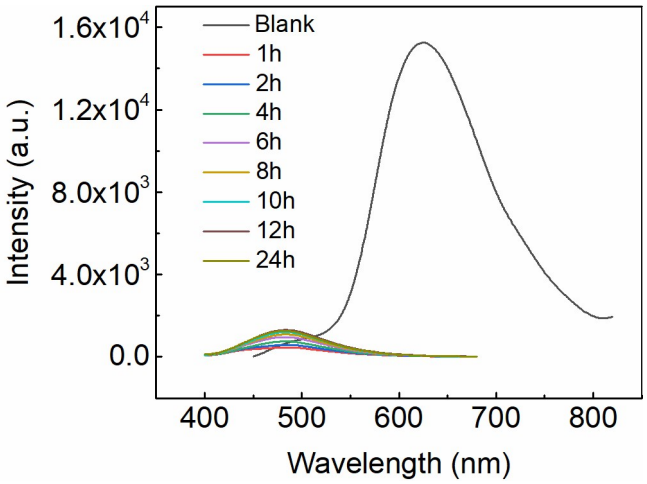

Figure S20. PL emission spectra for CD@BCOF-1 solution (100 mgL^{-1}) (λ_{ex} = 420 nm) after stirring for 24 hours (Blank). And the released CD particles was supervised from the supernatant after standing for different times (λ_{ex} = 380 nm).

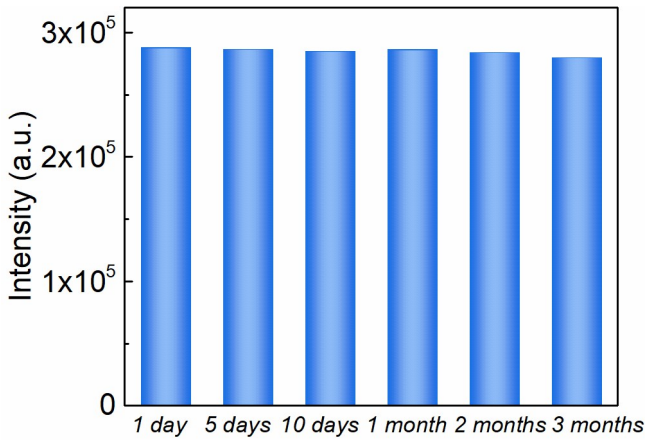

Figure S21. Stability of CD@BCOF-1 against different times.

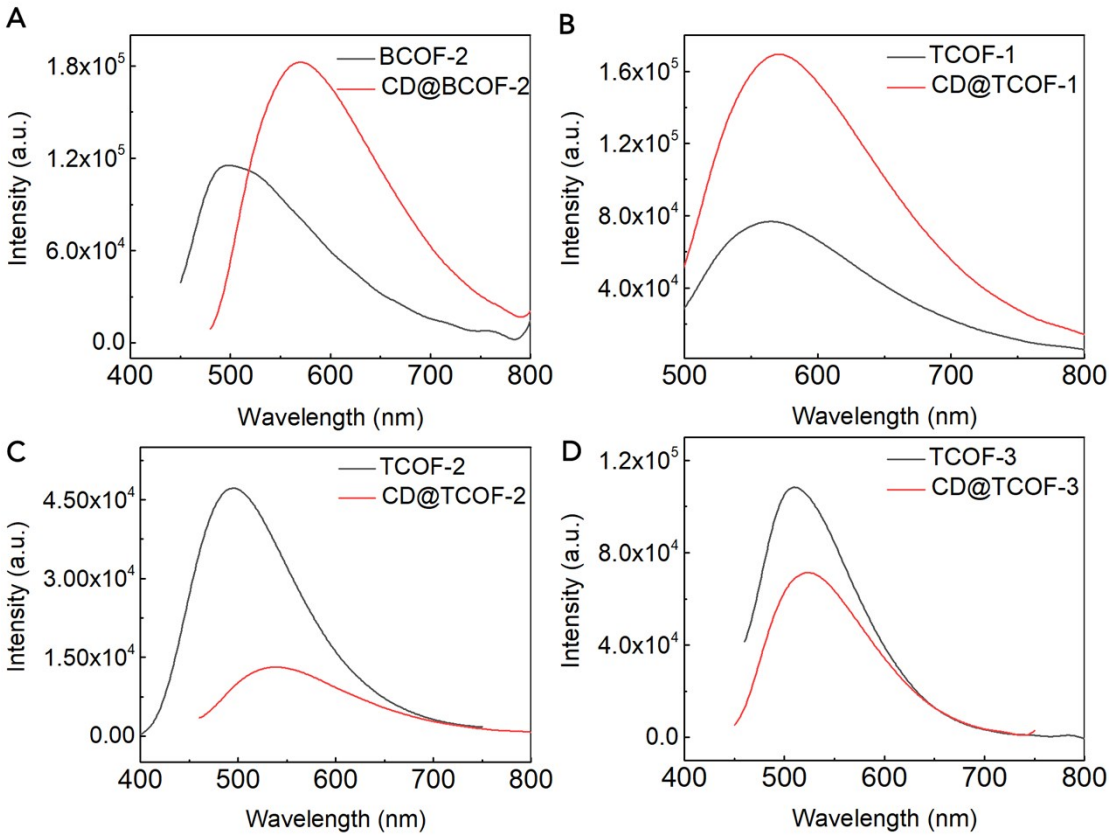

Figure S22. PL emission spectra for COFs and CD@COFs.

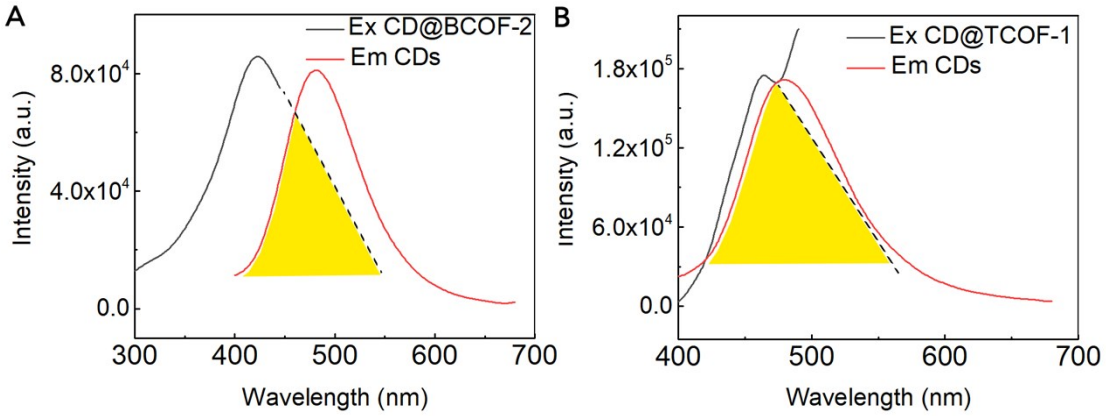

Figure S23. PL emission spectrum for CDs (λ_{ex} = 380 nm) and PL excitation spectra for CD@BCOF-2 (λ_{em} = 590 nm) and CD@TCOF-1 (λ_{em} = 590 nm).

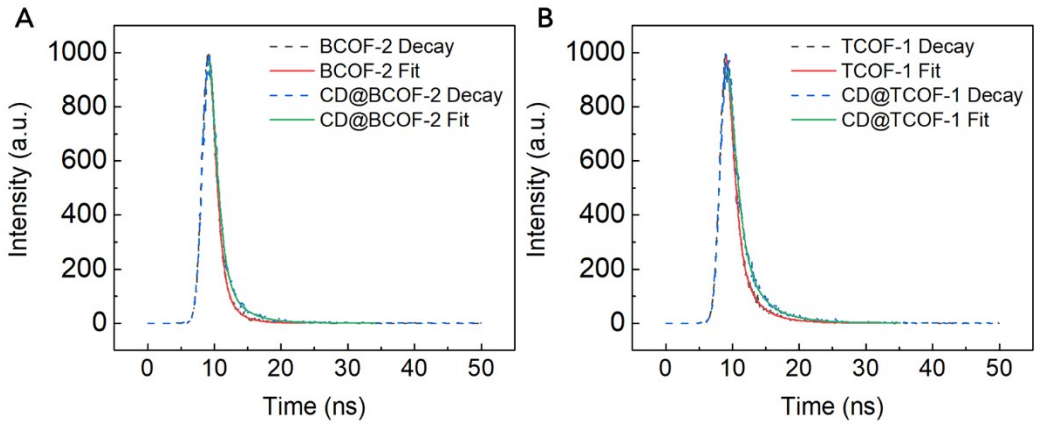

Figure S24. TRPL spectra and the corresponding fitting curves for CD@BCOF-2 and CD@TCOF-1, respectively, under 420 nm excitation.

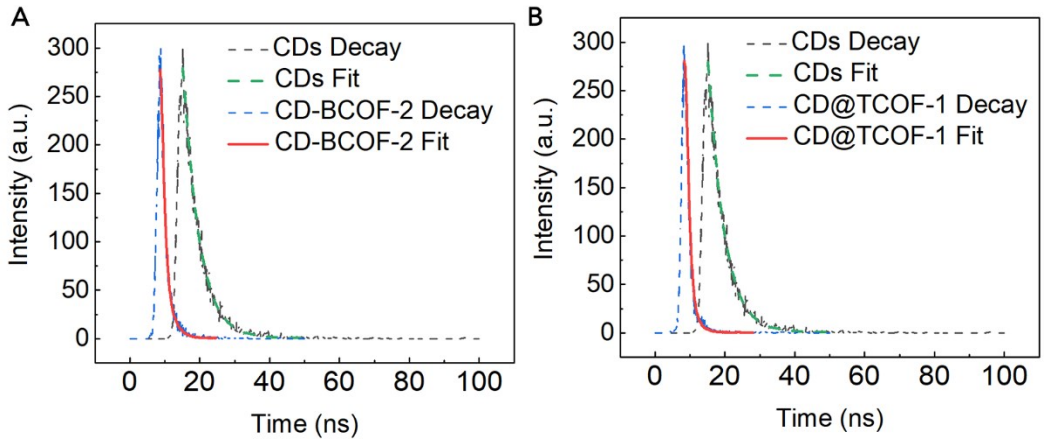

Figure S25. TRPL spectra and the corresponding fitting curves for CD@BCOF-2 and CD@TCOF-1, respectively, under 380 nm excitation.

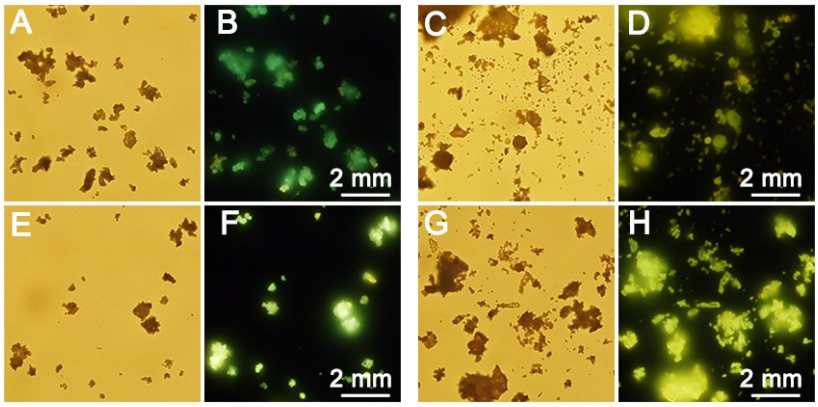

Figure S26. LSCM images for BCOF-2 (A and B), CD@BCOF-2 (E and F), TCOF-1 (C and D), and CD@TCOF-1 (G and H) under white light exposure and ultraviolet light (λ_{ex} = 365 nm).

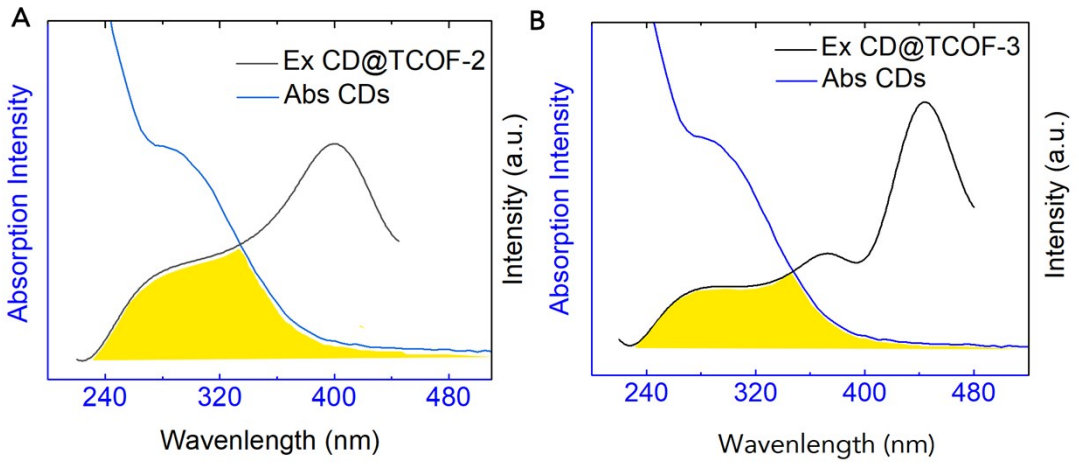

Figure S27. Absorption spectrum for CDs and PL excitation spectra for CD@TCOF-2 (λ_{em} = 500 nm) and CD@TCOF-3 (λ_{em} = 510 nm).

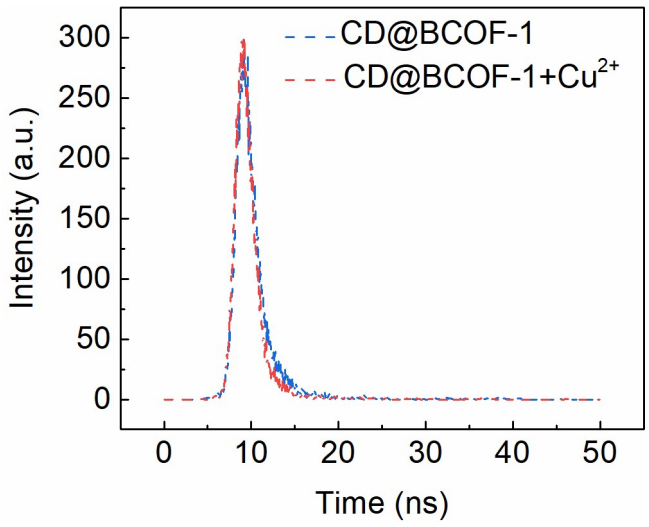

Figure S28. TRPL spectra for CD@BCOF-1 in the absence and presence of 1 mM Cu^{2+} ions.

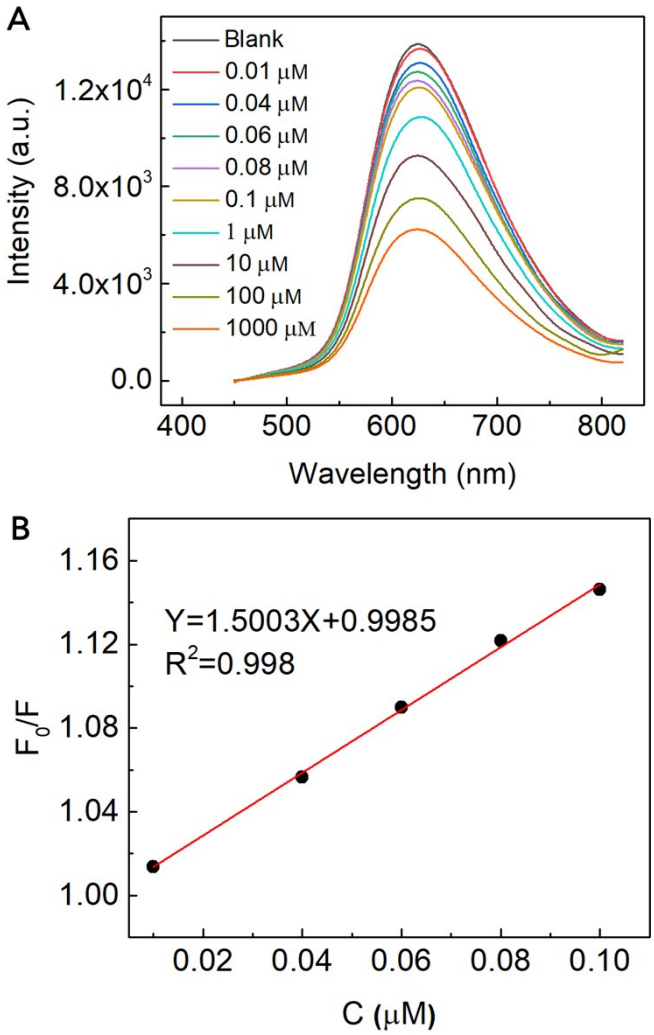

Figure S29. (a) Fluorescence emission spectra for the CD@BCOF-1 based sensor exposed to various concentrations of Cu^{2+} ions. (b) Fluorescence intensity versus the concentrations of Cu^{2+} ions.

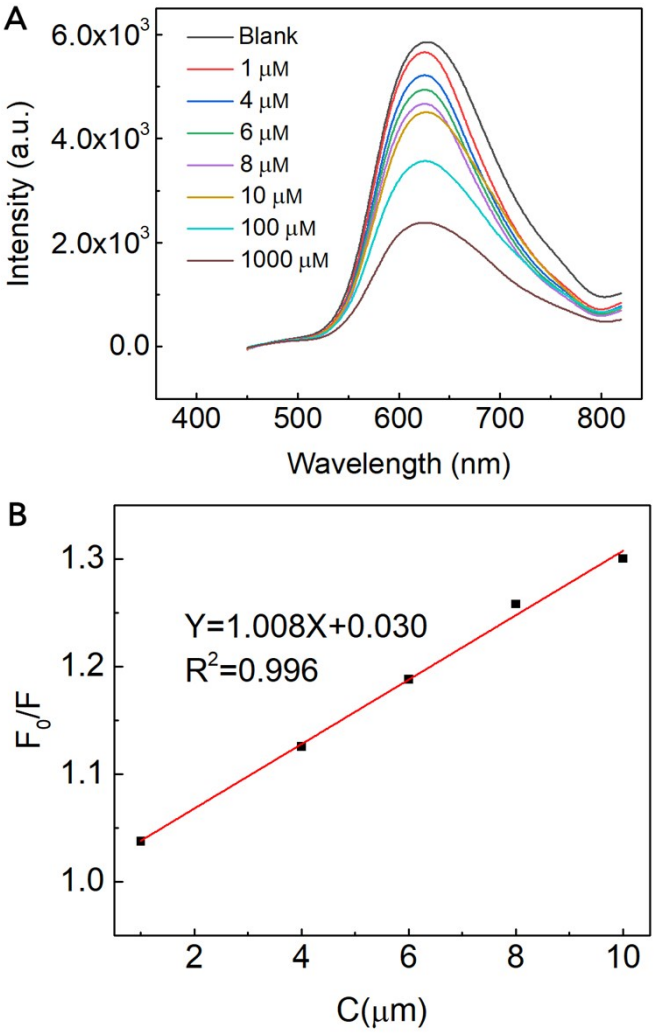

Figure S30. (a) Fluorescence emission spectra for the BCOF-1 based sensor exposed to various concentrations of Cu^{2+} ions. (b) Fluorescence intensity versus the concentrations of Cu^{2+} ions.

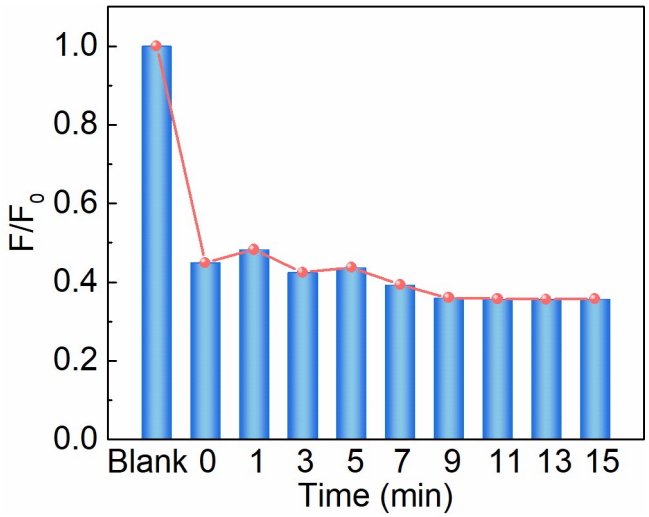

Figure S31. Fluorescence intensity of CD@BCOF-1 after contact with copper ions at different times

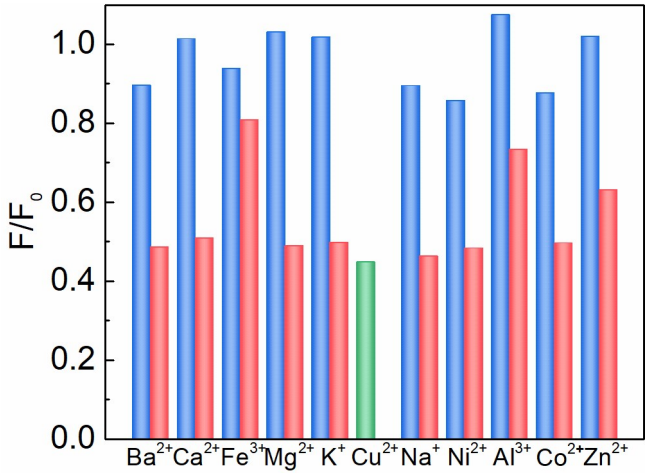

Figure S32. Selectivity of the CD@BCOF-1-based sensor for Cu^{2+} ions over other ions in water solution (blue column means CD@BCOF-1 in the presence of various ions; red column means CD@BCOF-1 in the presence of various ions and 10^{-3} M Cu^{2+} ions).

Table S1. CD@BCOF-1-X synthesis conditions and feed ratio.

COF	Mass (mg)	Sodium citrate (mg/ml)	Solvent (ml)	Temperature (℃)
5/64	10	1.56	0.5	300
5/32	10	3.12	0.5	300
5/16	10	6.25	0.5	300
5/8	10	12.5	0.5	300
5/4	10	25.0	0.5	300

Table S2. CHN elemental analysis of BCOF-1 and CD@BCOF-1.

	Weight% N	Weight% C	Weight% H
BCOF-1	27.50	62.80	3.93
	27.87	61.71	4.71
	26.94	63.95	3.88
average	27.43	62.82	4.17
CD@BCOF-1	25.43	60.43	4.01
	25.62	59.69	4.33
	24.88	60.11	3.84
average	25.31	60.07	4.06

Weight% O = 100% - weight% N - weight% C - weight% H

The calculated weight% O of BCOF-1 is 5.58%, and the weight% O of CD@BCOF-1 is 10.56%.

Table S3. Fitting parameters of time-resolved phosphorescence decay traces of COFs and CD@COFs (λ_{ex}=420 nm).

COF	t_1 (ns)	A_1 (%)	t_2 (ns)	A_2 (%)	t_{ave}
BCOF-1	0.572	100			0.572
CD@BCOF-1	1.369	100			1.359
BCOF-2	0.498	85.75	2.925	14.25	0.844
CD@BCOF-2	0.738	81.41	3.382	18.59	1.230
TCOF-1	0.792	73.44	3.330	26.56	1.466
CD@TCOF-1	1.015	63.56	3.795	36.44	2.028

Table S4. Fitting parameters of time-resolved phosphorescence decay traces for CDs and CD@COFs (λ_{ex}=380 nm, λ_{em}=480 nm).

Sample	t_1 (ns)	A_1 (%)	t_2 (ns)	A_2 (%)	t_{ave}
CDs	4.248	100			4.248
CD@BCOF-1	0.506	100			0.506
CD@BCOF-2	0.545	76.27	1.956	23.73	0.880
CD@TCOF-1	0.574	100			0.574